

ViTime: A Visual Intelligence-Based Foundation Model for Time Series Forecasting

Luoxiao Yang¹, Yun Wang², Xinqi Fan³, Israel Cohen⁴, Yue Zhao^{1*}, Zijun Zhang^{5*}

¹Xi'an University of Technology, China, ²Northwestern Polytechnical University, China,

³Manchester Metropolitan University, UK, ⁴Israel Institute of Technology, Israel

⁵City university of Hong Kong, Hong Kong SAR

* Corresponding author

Abstract

The success of large pretrained models in natural language processing (NLP) and computer vision (CV) has opened new avenues for constructing foundation models for time series forecasting (TSF). Traditional TSF foundation models rely heavily on numerical data fitting. In contrast, the human brain is inherently skilled at processing visual information, prefer predicting future trends by observing visualized sequences. From a biomimetic perspective, utilizing models to directly process numerical sequences might not be the most effective route to achieving Artificial General Intelligence (AGI). This paper proposes ViTime, a novel Visual Intelligence-based foundation model for TSF. ViTime overcomes the limitations of numerical time series data fitting by utilizing visual data processing paradigms and employs a innovative data synthesis method during training, called Real Time Series (RealTS). Experiments on a diverse set of previously unseen forecasting datasets demonstrate that ViTime achieves state-of-the-art zero-shot performance, even surpassing the best individually trained supervised models in some situations. These findings suggest that visual intelligence can significantly enhance time series analysis and forecasting, paving the way for more advanced and versatile models in the field. The code for our framework is accessible at <https://github.com/IkeYang/ViTime>.

Key words: Time Series Forecasting, Foundation Model, Visual Intelligence, Zero-shot, Data Synthesis

1 Introduction

Time series data are prevalent in various aspects of daily life, playing a crucial role in applications across numerous domains, such as weather forecasting [1], stock market analysis [2], traffic prediction [3], and healthcare monitoring [4]. Accurate analysis and prediction of time series data are essential for informed decision-making in these fields. Meanwhile, the emergence of large language models (LLMs) has highlighted the potential for creating general-purpose models capable of performing domain-specific tasks through zero-shot learning [5]. This breakthrough has generated considerable interest within the research community, leading to the development of foundational models for time series forecasting (TSF), which can significantly enhance the robustness and versatility of TSF, including recent TimesFM [6], ForecastPFN [7], and Time-LLM [8] etc.

Despite these advancements, existing foundational time series models encounter two significant challenges. First, similar to most TSF models, existing foundation models are trained by directly fitting numerical time series data, which suggests that the primary information carrier for these models is the numerical relationship within the temporal dimension. In contrast, humans tend to observe trends through

visual representations rather than processing numerical values directly. Research has shown that the human brain processes visual information more efficiently than numerical data. Pettersson [9] discovered that the human brain is more adept at processing visual information than numerical data. Similarly, Dondis [10] demonstrated that the visual cortex rapidly identifies patterns, shapes, and colors, making images and videos quicker to process than texts and numbers. These findings naturally lead to a hypothetical question: *On the path toward AGI, might employing visual intelligence for time series modeling be more effective than conventional numerical methods?*

Second, the training data of foundation models typically consist of large-scale real-world datasets [6], raising a critical question: *Can large real-world dataset comprehensively capture the diverse range of universal time series patterns?* Specifically, what foundational capabilities should a model possess to address a universal spectrum of time series problems?

To tackle these challenges, this paper proposes a novel visual intelligence-based time series foundation model, Visual Time Foundation Model (ViTime), aiming to pioneer a new research paradigm in time series foundation models from the perspective of visual intelligence. Additionally, we introduce an innovative time series data generation method, Real Time Series (RealTS), which categorizes foundational knowledge of time series analysis into "trend" and "periodicity" and synthesizes training data during ViTime's training. ViTime operates by transforming numerical time series into **binary images**, converting numerical temporal correlations into binary pixel spatial correlations. This methodology aligns with the brain's proficiency in processing time series data. Experimental results demonstrate that the proposed ViTime, when applied to various unseen datasets across different domains and resolutions, achieves state-of-the-art zero-shot results and, in some cases, surpasses the best individually trained supervised models. Moreover, with only 10% domain data fine-tuning, ViTime can achieve superior performance compared to the latest state-of-the-art supervised models using 100% domain data.

The main contributions of this work are highlighted as follows:

1. A Novel Visual Intelligence-Based Foundation Model for Time Series Analysis: A new visual intelligence-based framework for TSF foundation model, ViTime, is proposed, leveraging visual patterns instead of numerical data.

2. Innovative RealTS Data Generation Method: A novel data synthesis method, RealTS, is introduced, dividing the foundational knowledge of time series into "trend" and "periodicity" and generating training data to effectively pretrain ViTime.

3. Superior Performance: Comprehensive experimental results indicate that ViTime is a superior, more general, and more accurate foundation model, demonstrating its potential as a highly promising time series solution on the path to AGI.

2 Related work

2.1 Time series forecasting

Traditionally, TSF methods have been dominated by statistical models like the Autoregressive Integrated Moving Average (ARIMA) [11] and its extensions, including Seasonal ARIMA (SARIMA)

[12] and Vector ARIMA (VARIMA) [11]. While statistical models are appreciated for their simplicity and interpretability, they fall short in capturing the non-linear relationships and long-term dependencies inherent in real-world time series data.

In recent years, deep learning has made significant strides in TSF. Recurrent Neural Networks (RNNs) and their variants, such as Long Short-Term Memory (LSTM) networks and Gated Recurrent Units (GRUs), have shown superior capabilities in modeling complex temporal dependencies [13]. More recently, Transformers based models have gained attention for their ability to model long-range dependencies effectively. Models like Informer [14], Autoformer [15], and PatchTST [16] utilize self-attention mechanisms, setting new performance benchmarks in TSF.

2.2 Foundation model for time series forecasting

The TSF methods mentioned in Section 2.1 adopts a fully supervised learning paradigm, where specific models are trained on particular datasets. Recently, the advent of LLMs like GPT-3 and LLaMA-2, which aim to use a single, generalizable approach to predict across various datasets[5], has sparked interest in developing foundation models for TSF.

Research on foundation models for TSF is still in its early stages, and current approaches can be broadly categorized into LLM-based models, real-world dataset based models and synthesized dataset based models. The LLM-based models leverages the inference capabilities of LLMs for zero-shot TSF tasks, including TimeGPT-1 [17] and LLMTIME [8]. However, their accuracy heavily depends on the underlying capabilities of LLM, resulting in large, redundant, and less precise models. The real-world dataset based models aim training a foundation model on extensive real-world data to achieve zero-shot TSF, exemplified by Google's TimesFM [6]. Despite being one of the leading TSF foundation models, its reliance on real-world numerical time series data limits its robustness and coverage of various unseen time series patterns. The synthesized dataset based models employ synthetic data to train a foundation model, as demonstrated by ForecastPFN [7]. However, the uncontrollable nature of generated data patterns in real space often leads to lower accuracy for foundation models trained with synthetic data compared to those trained with real-world data.

2.3 Visual Intelligence assist model for time series forecasting

Research on visual intelligence assist TSF is relatively scarce. One of the earliest attempts is made by JP Morgan researchers [18], who investigated using images to predict financial data. However, this approach did not develop a systematic theoretical framework and lacked technical details, limiting its further development. In [19], the concept of using visual intelligence for TSF is systematically explored for the first time, establishing a theoretical framework that integrates visual intelligence for TSF. Nevertheless, the model proposed in [19] primarily focused on traditional supervised learning. There is still a gap in research about visual intelligence-based foundation model for TSF.

In this paper, we propose the Visual Intelligence-based model, ViTime, serving as a robust foundation model for TSF, which process time series data in the binary image-based time series metric space and training with high-quality synthetic data.

3 Method

3.1 Problem definition

The objective of this paper is to construct a synthesized dataset based foundation model for TSF, which is trained via synthesized time series data and subsequently applied to real-world time series data. Initially, we synthesize time series $s_{1:T+l}$ from a predefined distribution $P(D)$ to be used as training data, as shown in (1):

$$s_{1:T+l} \sim P(D) \quad (1)$$

where T and l denotes the length of the maximum lookback window and the maximum prediction length.

Following this, the proposed ViTime model learns from the synthesized data during the training phase and is tested on real data during the testing phase. The training problem can be mathematically formulated as follows:

$$\theta^* = \underset{\theta}{\operatorname{argmin}} L(\operatorname{ViTime}(s_{1:T}), s_{T:T+l}) \quad (2)$$

3.2 Overall architecture

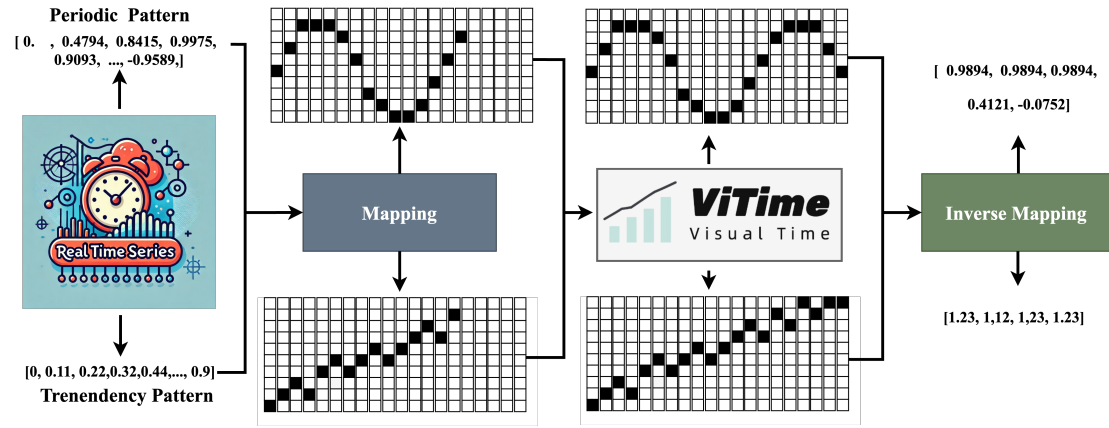


Fig. 1. The overall architecture of proposed ViTime.

Fig. 1 depicts the overall architecture of the proposed ViTime framework, which is composed of four key modules: the Real time series synthesis module, the mapping function, the proposed ViTime model, and the inverse mapping function. Initially, a novel time series data generation algorithm, Real Time Series (RealTS), is introduced in this paper, which categorizes the knowledge required for foundational time series models into two patterns: periodic pattern and trend pattern, and synthesizes numerical time series data accordingly. The generated numerical time series data are then mapped into a binary image by the mapping function, converting the numerical relationships of the time series data into spatial distribution relationships.

Next, the ViTime model operating within the binary image metric space is introduced, leveraging the historical distributions of the generated binary images to predict future trends. Consequently, the ViTime model transforms the TSF task into an image generation problem, enhancing predictive accuracy through the application of visual intelligence. Finally, the inverse mapping function is employed to convert the predicted binary image back into numerical time series data for further analysis.

In following sections, we will introduce each component of the ViTime framework in detail: RealTS,

Mapping Function, ViTime Model, and Inverse Mapping Function.

3.3 Real time series synthesis

A robust foundation model for TSF should integrate two essential types of time series variation knowledge: periodic pattern and trend pattern, which encompass the inherent patterns and directional changes in time series data. Real-world datasets, however, often lack representation of the full spectrum of these periodic and trend-based fluctuations, limiting the model's ability to generalize across different scenarios and effectively learn underlying dynamics.

To address this challenge, we propose a novel time series generation algorithm, RealTS. RealTS systematically generates synthetic time series data that exhibit diverse periodic and trend characteristics, providing a large dataset that captures a wide range of possible behaviors. The proposed RealTS can facilitate more comprehensive training of foundation models, exposing them to various patterns and improving their ability to generalize to unseen real-world data.

The RealTS algorithm probabilistically selects between generating periodic or trend-based time series. Given the total length L of synthesized time series, the algorithm selects the data prior hypothesis between periodic φ_p and trend-based φ_t patterns with a predefined probability (α). The distribution of generated time series $P(D)$ is defined as follows:

$$\begin{aligned} \mathbf{s}_L \sim P(D) = P(\mathbf{s}_L|L) = & \alpha \int P(\mathbf{s}_L|L, B_p)P(B_p|\varphi_p)P(\varphi_p)d\varphi_p \\ & + (1 - \alpha) \int P(\mathbf{s}_L|L, B_t)P(B_t|\varphi_t)P(\varphi_t)d\varphi_t \end{aligned} \quad (3)$$

where $P(\varphi)$ represents the prior probability of hypothesis φ ; $P(B|\varphi)$ is the likelihood of observing the data behavior B under hypothesis φ . The concept of data behavior B is introduced to further detail the generation behavior within different data modes.

We employ two distinct data behavior modes under periodic hypothesis φ_p :

Inverse Fast Fourier Transform Behavior (IFFTB): To ensure that the synthesized data adequately reflects the variation paradigms of real-world time series, we utilize IFFT as expressed in (4) to simulate the underlying behavior of real-world periodic time series:

$$P(\mathbf{s}_L|L, B_p)|_{B_p=IFFT} = \iint_{-\infty}^{\infty} N(\mathbf{A}_m; \boldsymbol{\mu}_{A_m}, \boldsymbol{\sigma}_{A_m}^2) N(\boldsymbol{\phi}; \boldsymbol{\mu}_p, \boldsymbol{\sigma}_p^2) \delta(\mathbf{s}_L - IFFT(\mathbf{A}_m, \boldsymbol{\phi}, L)) d\boldsymbol{\phi} d\mathbf{A}_m \quad (4)$$

where two empirical distribution of Fourier transform amplitudes and phases, $N(\mathbf{A}_m; \boldsymbol{\mu}_{A_m}, \boldsymbol{\sigma}_{A_m}^2)$ and $N(\boldsymbol{\phi}; \boldsymbol{\mu}_p, \boldsymbol{\sigma}_p^2)$, are maintained and δ denotes Dirac delta function. By sampling from empirical distributions, we can obtain the amplitude and Phase vector, which is then inversely transformed back to the time domain via *IFFT*.

Periodic Wave Behavior (PWB): This behavior generates data by superimposing multiple periodic waves. The data is modeled as a sum of sine, cosine and other periodic functions, f_{periodic} , with different frequencies and amplitudes:

$$P(\mathbf{s}_L|L, B_p)|_{B_p=PWB} = \iint_{-\infty}^{\infty} N\left(\mathbf{s}_L; \sum_{i=1}^{k_{PWB}} A_i f_{\text{periodic}}(\omega_i t), \boldsymbol{\sigma}_\epsilon^2\right) P(\mathbf{A}) P(\boldsymbol{\omega}) d\boldsymbol{\omega} d\mathbf{A} \quad (5)$$

where $P(\mathbf{A})$ and $P(\boldsymbol{\omega})$ denote predefined prior distributions of amplitudes and frequency; k_{PWB}

denotes the number of mixed periodic functions.

We also employ three distinct data behavior modes under trend data hypotheses φ_t :

Random Walk Behavior (RWB): The RWB models data as a stochastic process where each value is the previous value plus a random step:

$$P(s_i | s_{i-1}, L, B_p) |_{B_p=RWB} = N(0, \sigma^2) \quad (6)$$

Logistic Growth Behavior (LGB): The LGB models data with a logistic growth function, capturing the S-shaped growth pattern:

$$P(\mathbf{s}_L | L, B_p) |_{B_p=LGB} = \iint_{-\infty}^{\infty} N\left(\mathbf{s}_L; \frac{K}{1 + e^{-r(L-L_0)}}, \sigma_\epsilon^2\right) P(K)P(r) dK dr \quad (7)$$

where $P(K)$ and $P(r)$ denote predefined prior distributions of S-shaped function hyperparameters.

Trend Wave Data Behavior (TWDB): The TWDB combines linear trends with periodic fluctuations:

$$= \iint_{-\infty}^{\infty} N\left(\mathbf{s}_L; aL + b + \sum_{i=1}^{k_{TWDB}} A_i f_{\text{periodic}}(\omega_i t), \sigma_\epsilon^2\right) P(a)P(b)\mathbf{P}(\mathbf{A})\mathbf{P}(\boldsymbol{\omega}) da db d\mathbf{A} d\boldsymbol{\omega} \quad (8)$$

where $P(a)$, $P(b)$, $\mathbf{P}(\mathbf{A})$ and $\mathbf{P}(\boldsymbol{\omega})$ denote predefined prior distributions of hyperparameters.

During synthesis process, we employ various data augmentation techniques to enhance the diversity and robustness of synthetic data, including Multiple period replication, which repeats the generated periodic data over multiple cycles to capture long-term periodic patterns; Data flipping; Convolution smoothing and detrending, which remove underlying trends from the data to isolate periodic components, make it easier for the model to learn these patterns; Data perturbation, which introduces sudden changes or anomalies into the data, simulating real-world disturbances and improving the model's ability to handle unexpected variations, etc..

Fig. 2 illustrates the synthesized data generated by RealTS, demonstrating its ability to produce a wide range of time series with various periodic patterns and enabling the model to acquire extensive knowledge of periodicity and trends. Detailed settings for predefined prior/empirical distributions are provided in Appendix I.

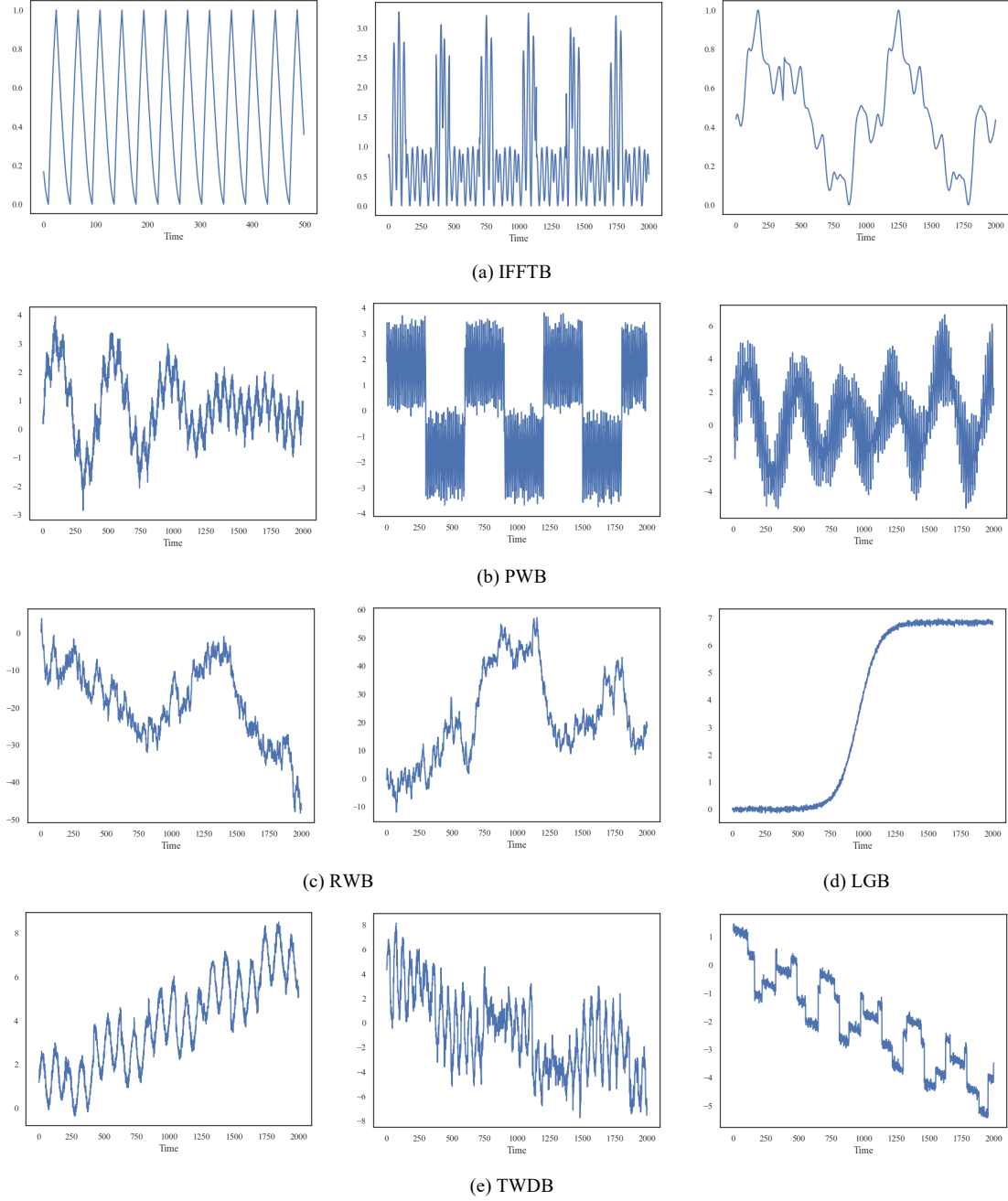


Fig. 2. Illustrations of synthesized data generated by RealTS

3.4 Binary image based time series metric space

In ViTime, time series are fed and operated with a binary image form, leveraging a binary image-based time series metric space proposed in [19], as described in Definition 1.

Definition 1: Binary image-based time series metric space. The binary image-based time series metric space is defined as a group (V, d) , where V is a set of elements defined in equation (9) and $d: V \times V \rightarrow \mathbb{R}$ is a distance function based on the Earth Mover's Distance (EMD), defined in (10).

$$\mathcal{V} = \{v \in R^{c \times h \times L} \mid v_{i,j,k} \in \{0,1\}, i \in [c], j \in [h], k \in [L], \sum_{j=1}^h v_{i,j,k} = 1\} \quad (9)$$

$$d(v_1, v_2) = \int_{i=1}^c \int_{k=1}^L \inf_{\gamma \in \Pi(v_1^{i:1:h,k}, v_2^{i:1:h,k})} \mathbb{E}_{x,y \sim \gamma} \|x - y\|_1 dk di \quad (10)$$

where c represents the number of variates, L is the length of the time series, and h is the resolution of V .

To enable the transition from numerical time-series values to the binary image-based metric space, we introduce mapping and inverse mapping functions as follows. Let $\mathcal{S} = \{s \in R^{c \times L} | s_{i,k} \in R\}$ represent the numerical value space of time series. The Time-Series-to-Image mapping function $f: \mathcal{S} \rightarrow \mathcal{V}$ and the Image-to-Time-Series inverse mapping function $f^{-1}: \mathcal{V} \rightarrow \mathcal{S}$ can be defined as follows:

$$\begin{aligned} \mathbf{v}_{i,1:h,k} &= \mathbf{f}(s_{i,k}) = \langle f_1(s_{i,k}), f_2(s_{i,k}), \dots, f_h(s_{i,k}) \rangle, \quad f_j(s_{i,k}) \\ &= \begin{cases} 1, & s_{i,k} \geq MS, j = h \\ 1, & s_{i,k} \leq MS, j = 1 \\ 1, & j = \left\lfloor \frac{s_{i,k} + MS}{\frac{2MS}{h}} \right\rfloor, j \in [h] \\ 0, & \text{else} \end{cases} \end{aligned} \quad (11.1)$$

$$\begin{aligned} s_{i,k} &= \mathbf{f}^{-1}(\mathbf{v}_{i,1:h,k}) \\ &= \sum_{j=1}^h \left((j - 0.5) \times \frac{2MS}{h} - MS \right) \times v_{i,j,k} \end{aligned} \quad (11.2)$$

where $MS > 0$ denotes the maximum scale of \mathcal{V} . Before mapping, zero-score normalization is typically applied to the numerical time series $s_{i,k}$ to standardize the scale.

Given that the numerical time series data synthesized by RealTS are one-channel time series, i.e. $\mathbf{s}_L \in R^L \in R^{1 \times L}$, thus the corresponding $\mathbf{v}_L \in R^{1 \times h \times L}$ is obtained via (12):

$$\mathbf{v}_L = \mathbf{f}(\mathbf{s}_L) \quad (12)$$

3.5 The proposed ViTime model

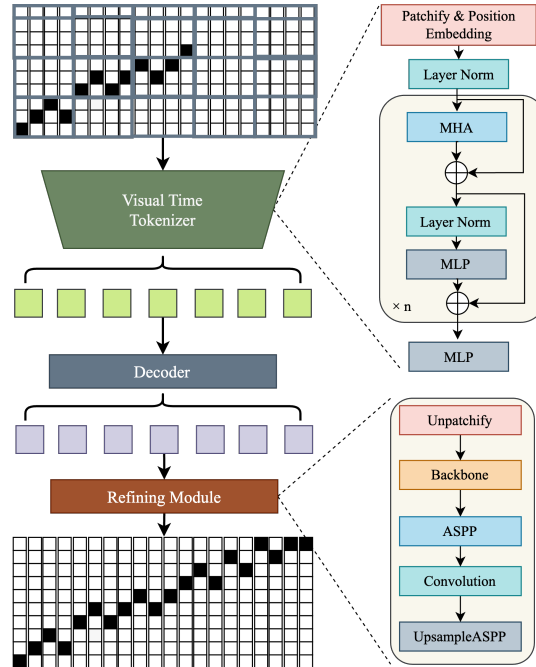


Fig. 3. Model framework

Fig. 3 depicts the framework of the proposed ViTime model, which comprises three networks: the Visual Time Tokenizer, the Decoder, and the Refining Module. Initially, temporal masking is applied to the mapped binary image, ensuring the temporal information is not disclosed. The masked binary image

is then fed into the Visual Time Tokenizer and outputs embedded tokens. These tokens are subsequently decoded by the Decoder, resulting in the initial prediction. Finally, to enhance the generative quality of patch junctions, a Refining Module is employed to output the final binary image prediction.

Visual Time Tokenizer. The primary role of the Visual Time Tokenizer is to segment masked binary image into multiple patches, integrate positional encoding, and map these patches into the feature space. By leveraging the Vision Transformer (ViT) [20] architecture, the module captures spatial relationships between patches, thereby transforming temporal dependencies of the time series into spatial dependencies within the pixel value space.

Decoder. The Decoder translates the tokenized patches back into the original binary pixel metric space, providing an initial prediction where the ViT architecture is adopted as well.

Refining Module. The transformer architecture in the Decoder can result in discontinuities at the patch junctions, which may affect the accuracy of inverse mapping process. To address this issue, the Refining Module building with CNNs is employed. Initially, tokens decoded by Decoder are unpatched and fed into a CNN-based backbone. Next, an Atrous Spatial Pyramid Pooling (ASPP) [21] module is employed to expand model receptive field. Finally, the output is upsampled to the original binary pixel metric space, generating the final binary image prediction result.

The modeling process of ViTime can be expressed in (13):

$$\mathbf{v}'_L = ViTime(\mathbf{v}_L \odot \mathbf{M}_L) \quad (13)$$

where \mathbf{M}_L denotes temporal masks.

3.6 Training details

We incorporate following technique details during training.

Data normalization. To ensure ViTime can effectively capture patterns involving sudden changes, an in-sequence data normalization based on L2 normalization is implemented. By normalizing each sequence within the data sequence, the model can pay more attention to abrupt variations. The normalization process is defined as follows:

$$\mathbf{S}_L = \frac{\mathbf{S}_L - \text{mean}(\|\mathbf{S}_{1:T}\|_2)}{\text{std}(\mathbf{S}_{1:T})} \quad (14)$$

Temporal resolution enhancement. To improve the temporal resolution in the binary image metric space, the input sequence is first linearly interpolated to twice its original length ($2L$), so that, the granularity of the temporal dimension is increase. Moreover, due to the inherent sparsity of the binary image space, most patches exhibit low-level information density. To improve the information density, Gaussian blurring is applied to the input binary images before fed into ViTime, thereby reducing sparsity and enhancing information density.

Loss function. The loss function employed in this study is defined as follows:

$$\mathcal{L} = d(\mathbf{v}'_L, \mathbf{v}_L) + \alpha KLD(\mathbf{v}'_L, \mathbf{v}_L) \quad (15)$$

where d denotes distance function defined in (10), KLD denotes Kullback–Leibler divergence and α is the hyperparameter balance quantity between d and KLD .

4 Computational experiments

4.1 Experimental Configuration

4.1.1 Datasets

Seven popular publicly accessible datasets, Electricity, Traffic, Weather, ETTh1, ETTh2, ETTm1 and ETTm2 [15] are employed in computational section to validate the effectiveness of the proposed method.

4.1.2 Model setup

The ViTime model is developed using data sequences synthesized by RealTS. During each training epoch, 20,000 sequences are randomly generated. Detailed RealTS parameters setting are provided in Appendix I. After training, zero-shot testing and fine-tuning are implemented accordingly. For multivariate time series, a channel-independent strategy [16] is applied, predicting each variable separately before combining them to form the final multivariate forecast.

The default parameters for ViTime model are set as follows: $h = 128$, $MS = 3.5$, maximum lookback window $T = 512$, and maximum prediction length $l = 720$. Gaussian blur with a kernel size of (31,31) is applied to the binary image to facilitate faster convergence. The detailed structural design of the Visual Time Tokenizer, the Decoder, and the Refining Module is outlined in Appendix II.

4.1.3 Evaluation Metrics

Foundational models for TSF trained on real-world data can suffer from test set leakage issue. To address this issue and ensure a fair experimental comparison, two metrics are proposed for zero-shot evaluation: Rescale-MAE (ReMAE) and Rescale-MSE (ReMSE). The primary concept of ReMAE/ReMSE involves rescaling the test dataset with different time resolutions, For example, the original test time series of length T is rescaled to βT using the time series interpolation (TSI) method, as shown in (16).

$$S_{\beta T} = TSI(S_T, \text{rescaling factor} = \beta) \quad (16)$$

The formulas for ReMAE and ReMSE are provided below:

$$MSE(S'_{\beta T}, S_{\beta T}) = \frac{\|S'_{\beta T} - S_{\beta T}\|_2^2}{\beta T} \quad (17.1)$$

$$MAE(S'_{\beta T}, S_{\beta T}) = \frac{\|S'_{\beta T} - S_{\beta T}\|_1}{\beta T} \quad (17.2)$$

$$ReMSE = \frac{\sum_{\beta \in B} MSE(S'_{\beta T}, S_{\beta T})}{len(B)}, B = [0.5, 0.66, 1, 1.5, 2] \quad (17.3)$$

$$ReMAE = \frac{\sum_{\beta \in B} MAE(S'_{\beta T}, S_{\beta T})}{len(B)}, B = [0.5, 0.66, 1, 1.5, 2] \quad (17.4)$$

Table I. Zero-shot forecasting result of considered methods. The best results are **bolded**, the second best are underlined and the result better than supervised PatchTST are marked with purple.

| Method | | ViTime-1072 | | ViTime | | PatchTST-ZS | | TimesFM | | PatchTST | |
|---------------|-----|--------------|--------------|--------------|--------------|-------------|--------|-----------------|--------------|-----------------|--------------|
| Training data | | RealTS | | RealTS | | RealTS | | Real world data | | Real world data | |
| Supervision | | Zero-shot | | Zero-shot | | Zero-shot | | Zero-shot | | Supervised | |
| Metric | | ReMS | ReMA | ReMS | ReMAE | ReMS | ReMA | ReMS | ReMA | ReMS | ReMA |
| | | E | E | E | | E | E | E | E | E | E |
| Electricity | 96 | 0.216 | 0.297 | 0.216 | <u>0.302</u> | 1.336 | 0.896 | 0.269 | 0.338 | <i>0.121</i> | <i>0.216</i> |
| | 192 | 0.229 | 0.308 | <u>0.232</u> | <u>0.316</u> | 1.425 | 0.924 | 0.322 | 0.375 | <i>0.139</i> | <i>0.234</i> |
| | 336 | 0.244 | 0.320 | <u>0.255</u> | <u>0.333</u> | 1.443 | 0.929 | 0.381 | 0.414 | <i>0.156</i> | <i>0.251</i> |
| | 720 | 0.296 | 0.355 | <u>0.334</u> | <u>0.383</u> | 1.451 | 0.9317 | 0.496 | 0.488 | <i>0.194</i> | <i>0.286</i> |
| Average | | 0.246 | 0.320 | <u>0.259</u> | <u>0.334</u> | 1.414 | 0.920 | 0.367 | 0.404 | <i>0.153</i> | <i>0.247</i> |
| Traffic | 96 | 0.665 | 0.357 | <u>0.691</u> | <u>0.389</u> | 1.964 | 0.975 | 0.771 | 0.459 | <i>0.327</i> | <i>0.242</i> |
| | 192 | 0.658 | 0.354 | <u>0.684</u> | <u>0.390</u> | 2.073 | 1.008 | 0.818 | 0.495 | <i>0.342</i> | <i>0.249</i> |
| | 336 | 0.660 | 0.357 | <u>0.709</u> | <u>0.401</u> | 2.071 | 1.011 | 0.878 | 0.524 | <i>0.359</i> | <i>0.259</i> |
| | 720 | 0.725 | 0.391 | <u>0.818</u> | <u>0.448</u> | 2.105 | 1.012 | 1.033 | 0.595 | <i>0.387</i> | <i>0.274</i> |
| Average | | 0.677 | 0.365 | <u>0.726</u> | <u>0.407</u> | 2.053 | 1.002 | 0.875 | 0.518 | <i>0.353</i> | <i>0.256</i> |
| Weather | 96 | <u>0.179</u> | 0.210 | 0.178 | <u>0.215</u> | 0.836 | 0.561 | 0.171 | <u>0.215</u> | <i>0.146</i> | <i>0.197</i> |
| | 192 | 0.233 | 0.258 | <u>0.234</u> | <u>0.262</u> | 0.922 | 0.588 | 0.236 | 0.273 | <i>0.195</i> | <i>0.244</i> |
| | 336 | 0.285 | 0.295 | <u>0.291</u> | <u>0.303</u> | 0.938 | 0.592 | 0.303 | 0.327 | <i>0.241</i> | <i>0.281</i> |
| | 720 | 0.352 | 0.341 | <u>0.369</u> | <u>0.355</u> | 0.945 | 0.594 | 0.427 | 0.411 | <i>0.307</i> | <i>0.328</i> |
| Average | | 0.262 | 0.276 | <u>0.268</u> | <u>0.284</u> | 0.910 | 0.584 | 0.284 | 0.307 | <i>0.222</i> | <i>0.263</i> |
| ETTh1 | 96 | <u>0.465</u> | <u>0.436</u> | 0.490 | 0.446 | 1.398 | 0.877 | 0.409 | 0.413 | <i>0.365</i> | <i>0.396</i> |
| | 192 | 0.478 | 0.448 | 0.514 | <u>0.454</u> | 1.490 | 0.908 | <u>0.486</u> | 0.458 | <i>0.414</i> | <i>0.431</i> |
| | 336 | 0.504 | 0.467 | <u>0.533</u> | <u>0.471</u> | 1.507 | 0.912 | 0.535 | 0.488 | <i>0.457</i> | <i>0.461</i> |
| | 720 | 0.570 | 0.513 | <u>0.620</u> | <u>0.521</u> | 1.511 | 0.914 | 0.623 | 0.545 | <i>0.550</i> | <i>0.506</i> |
| Average | | 0.504 | 0.466 | 0.539 | <u>0.473</u> | 1.477 | 0.903 | <u>0.513</u> | 0.476 | <i>0.447</i> | <i>0.449</i> |
| ETTh2 | 96 | 0.252 | 0.323 | <u>0.275</u> | <u>0.335</u> | 1.032 | 0.752 | <u>0.265</u> | <u>0.324</u> | <i>0.290</i> | <i>0.349</i> |
| | 192 | 0.285 | 0.351 | <u>0.314</u> | <u>0.361</u> | 1.115 | 0.782 | <u>0.316</u> | <u>0.362</u> | <i>0.347</i> | <i>0.390</i> |
| | 336 | 0.351 | 0.395 | <u>0.362</u> | <u>0.400</u> | 1.115 | 0.781 | <u>0.365</u> | <u>0.401</u> | <i>0.372</i> | <i>0.414</i> |
| | 720 | 0.431 | 0.450 | <u>0.450</u> | <u>0.462</u> | 1.122 | 0.783 | 0.472 | 0.476 | <i>0.451</i> | <i>0.469</i> |
| Average | | 0.330 | 0.380 | <u>0.350</u> | <u>0.390</u> | 1.096 | 0.775 | <u>0.355</u> | <u>0.391</u> | <i>0.365</i> | <i>0.406</i> |
| ETTm1 | 96 | 0.478 | 0.414 | <u>0.478</u> | <u>0.417</u> | 1.215 | 0.773 | 0.576 | 0.454 | <i>0.296</i> | <i>0.347</i> |
| | 192 | 0.501 | 0.431 | <u>0.504</u> | <u>0.434</u> | 1.309 | 0.801 | 0.608 | 0.479 | <i>0.338</i> | <i>0.374</i> |
| | 336 | 0.517 | 0.444 | <u>0.546</u> | <u>0.458</u> | 1.329 | 0.808 | 0.705 | 0.517 | <i>0.381</i> | <i>0.398</i> |
| | 720 | 0.558 | 0.469 | <u>0.634</u> | <u>0.503</u> | 1.327 | 0.807 | 0.792 | 0.563 | <i>0.421</i> | <i>0.423</i> |
| Average | | 0.514 | 0.440 | <u>0.541</u> | <u>0.453</u> | 1.295 | 0.797 | 0.670 | 0.503 | <i>0.359</i> | <i>0.386</i> |
| ETTm2 | 96 | 0.218 | 0.293 | 0.213 | 0.282 | 0.749 | 0.593 | <u>0.214</u> | <u>0.284</u> | <i>0.174</i> | <i>0.262</i> |
| | 192 | 0.270 | <u>0.330</u> | 0.273 | 0.326 | 0.823 | 0.618 | 0.295 | 0.330 | <i>0.227</i> | <i>0.301</i> |
| | 336 | 0.316 | 0.360 | <u>0.330</u> | <u>0.363</u> | 0.817 | 0.617 | 0.368 | 0.377 | <i>0.279</i> | <i>0.336</i> |
| | 720 | 0.395 | 0.409 | <u>0.417</u> | <u>0.416</u> | 0.829 | 0.621 | 0.465 | 0.443 | <i>0.348</i> | <i>0.382</i> |
| Average | | 0.300 | <u>0.348</u> | <u>0.308</u> | 0.347 | 0.805 | 0.612 | 0.336 | 0.359 | <i>0.257</i> | <i>0.320</i> |

4.2 Zero-shot Evaluation

To evaluate the zero-shot performance of our model, we consider two leading state-of-the-art TSF models: TimesFM [6], introduced by Google Research in April 2024 and acknowledged as the most powerful open-source foundational time series model, and PatchTST[16], a well-established model in supervised and transfer learning for TSF over the past two years. For fair comparison, all models employ lookback length of 512 to forecast future sequences of lengths 96, 192, 336, 720. For the ViTime-1072 model, we used longer lookback length, 1072, to test its peak accuracy. PatchTST-ZS utilizes the same training data as ViTime, generated by RealTS, whereas TimesFM is pre-trained on extensive real-world datasets before zero-shot testing. Additionally, we incorporated a fully supervised PatchTST model, which trained distinct models on various datasets to serve as the benchmark for maximum achievable

accuracy through supervision.

Table I reports the zero-shot experimental results. The proposed ViTime-1072 model achieves the highest accuracy in almost all experiments. When using the same input sequence length as the other baseline models, ViTime consistently ranks best across almost all datasets and prediction lengths, significantly outperforming TimesFM. Notably, ViTime’s accuracy in some cases even surpasses that of the fully supervised PatchTST model, showcasing the superiority of the proposed ViTime. The comparative results between ViTime and PatchTST-ZS, both trained on RealTS-generated data, suggest that modeling TSF tasks from a visual intelligence perspective can significantly enhance model robustness and accuracy, which further validates the rationale behind the ViTime framework's design from a visual intelligence perspective.

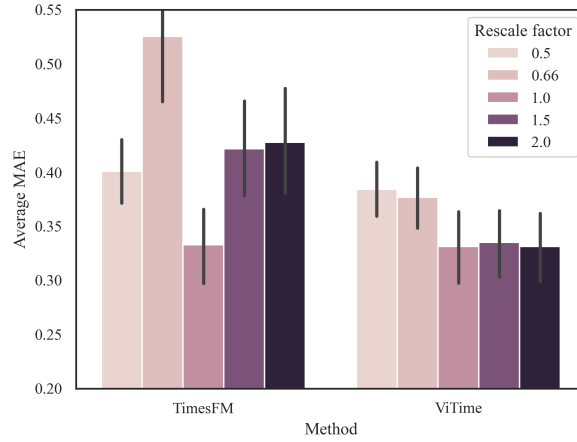


Fig. 4. Model performance under different rescaling factors.

Fig. 4 depicts the testing accuracy of the proposed ViTime versus TimesFM across different rescaling factors in (17). TimesFM, a foundational model trained on real data, achieve high accuracy at rescaling factor=1 but performs poorly at other factors, indicating potential data leakage issues in the training set. In contrast, ViTime consistently delivers robust prediction results across all rescaling factors, demonstrating its superior performance and adaptability as a foundational TSF model. Additional visualization results with benchmarks are offered in Appendix III.

4.3 Fine-tune Evaluation

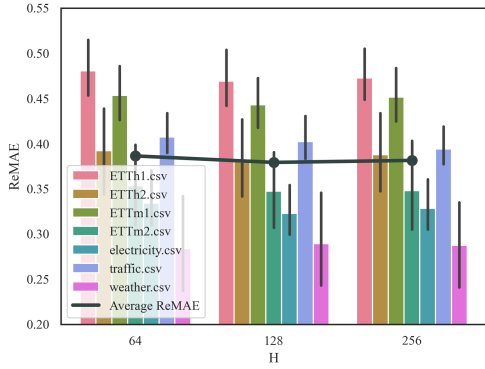
To further evaluate the performance of ViTime, we conduct a series of fine-tuning experiments in this section. Foundational models such as TimesFM [6], GPT4TS [22], and TIME-LLM [8] are fine-tuned using 10% of the training data. We also considered recent SOTA supervised TSF models, including SiMBA [23], TIMESNET [24], and PatchTST [16], using 100% of the training data as reported in their papers. The proposed ViTime is fine-tuned with both 10% and 100% of the training data, with results presented in Table II.

It is observable that the proposed ViTime, when fine-tuned with 10% of the training data, outperforms the latest supervised models that were trained on 100% of the data. Furthermore, when fine-tuned with 100% of the data, ViTime's prediction accuracy greatly surpasses all existing models, further demonstrating its effectiveness. Detailed results of the fine-tuning experiments are provided in the Appendix IV.

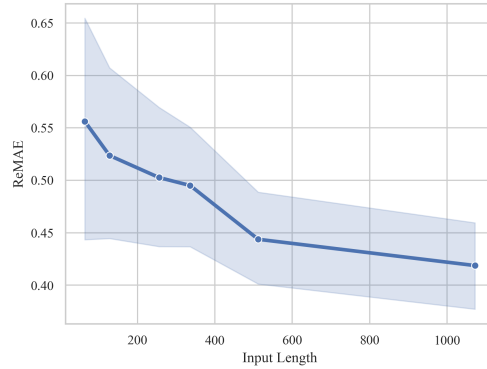
Table II. Fine-tuning forecasting result of considered methods. The best results are **bolded** and the second best are underlined.

| Method | Data proportion | ETTh1 | ETTh2 | ETTh1 | ETTh2 |
|-------------------|-----------------|--------------|--------------|--------------|--------------|
| TimesFM(FT) | 10% | 0.426 | 0.410 | 0.388 | 0.334 |
| GPT4TS(FT) | 10% | 0.525 | 0.421 | 0.441 | 0.335 |
| TIME-LLM(FT) | 10% | 0.522 | 0.394 | 0.427 | 0.323 |
| <u>ViTime(FT)</u> | <u>10%</u> | <u>0.424</u> | <u>0.372</u> | <u>0.378</u> | <u>0.316</u> |
| PatchTST | 10% | 0.542 | 0.431 | 0.466 | 0.343 |
| PatchTST | 100% | 0.434 | 0.381 | 0.382 | 0.317 |
| SiMBA | 100% | 0.433 | 0.393 | 0.396 | 0.327 |
| TIMESNET | 100% | 0.450 | 0.427 | 0.406 | 0.332 |
| ViTime(FT) | 100% | 0.408 | 0.349 | 0.367 | 0.300 |

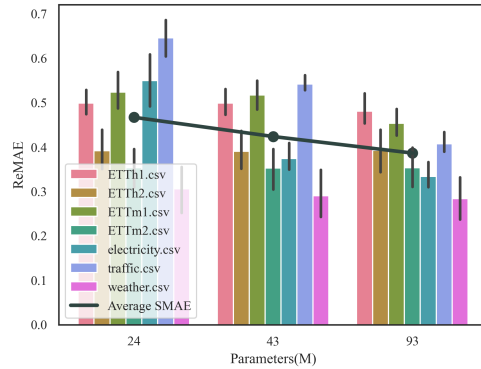
4.4 Ablation



(a) Forecasting performance varying with h



(b) Forecasting performance varying with the length of lookback window.



(c) Forecasting performance across different model size. The model size of ViTime used in computational experiments is 93M parameters version.

Fig. 5. Ablation studies with zero-shot forecasting.

In this section, we perform several ablation studies to gain deeper insights of model configuration. The results of ablation experiments are reported in Fig. 5. Fig. 5a depicts the influence of varying spatial resolutions (h) on model accuracy. Although increasing h slightly improves the prediction results, the associated computational cost increases exponentially. Thus, setting h to 128 is a more economical and

efficient choice. Fig. 5b illustrates the effect of different lookback window lengths (T) on prediction accuracy. It is evident that a longer lookback window length significantly enhances the model's prediction accuracy. Fig. 5c reports the prediction accuracy across different model sizes. The data shows that models with more parameters tend to perform better. Notably, the proposed ViTime achieves exceptional performance with only 93M parameters, demonstrating its efficiency and effectiveness.

5 Conclusion

In this paper, we introduced ViTime, a Visual Intelligence-based foundation model for TSF, along with a novel data generation method, RealTS. Our approach was designed to address the inherent limitations of traditional numerical data fitting models by leveraging visual processing capabilities, which align more closely with the human brain's strengths in handling visual information. The proposed ViTime framework transformed numerical time series data into a binary image, enabling the application of visual intelligence techniques to analyze and predict time series trends. Moreover, the proposed RealTS algorithm could systematically generate diverse synthetic time series data, encapsulating essential periodic and trend characteristics and providing enough knowledge for training ViTime model.

Extensive experimental evaluations demonstrated that ViTime could achieve state-of-the-art zero-shot performance. Meanwhile, the fine-tuning experiments indicated the proposed ViTime could outperform recent state-of-the-art fully supervision models even when trained with 10% data, confirming the benefits of visual intelligence for time series analysis. We believe that the proposed ViTime can provide significant insights for AGI processing time series from a methodological perspective.

Reference

- [1]. Yang, L., Zheng, Z., & Zhang, Z. (2021). An improved mixture density network via wasserstein distance based adversarial learning for probabilistic wind speed predictions. *IEEE Transactions on Sustainable Energy*, 13(2), 755-766
- [2]. Lin, W. Y., Hu, Y. H., & Tsai, C. F. (2011). Machine learning in financial crisis prediction: a survey. *IEEE Transactions on Systems, Man, and Cybernetics, Part C (Applications and Reviews)*, 42(4), 421-436.
- [3]. Liu C, Yang S, Xu Q, et al. Spatial-temporal large language model for traffic prediction[J]. *arXiv preprint arXiv:2401.10134*, 2024.
- [4]. Chen, M., Hao, Y., Hwang, K., Wang, L., & Wang, L. (2017). Disease prediction by machine learning over big data from healthcare communities. *Ieee Access*, 5, 8869-8879.
- [5]. Alec Radford, Jeffrey Wu, Rewon Child, David Luan, Dario Amodei, Ilya Sutskever, et al. Language models are unsupervised multitask learners. *OpenAI blog*, 1(8):9, 2019.
- [6]. Das A, Kong W, Sen R, et al. A decoder-only foundation model for time-series forecasting[J]. *arXiv preprint arXiv:2310.10688*, 2023.
- [7]. Dooley S, Khurana G S, Mohapatra C, et al. Forecastpfn: Synthetically-trained zero-shot forecasting[J]. *Advances in Neural Information Processing Systems*, 2024, 36.
- [8]. Jin M, Wang S, Ma L, et al. Time-llm: Time series forecasting by reprogramming large language models[J]. *arXiv preprint arXiv:2310.01728*, 2023.
- [9]. R. Pettersson, "Visual information". *Educational Technology*, 1993.
- [10]. Donis A .Dondis, "A primer of visual literacy". *Mit Press*, 1974.
- [11]. Vu K M. The ARIMA and VARIMA time series: Their modelings, analyses and applications[M]. *AuLac Technologies Inc.*, 2007.

- [12]. Dabral P P, Murry M Z. Modelling and forecasting of rainfall time series using SARIMA[J]. *Environmental Processes*, 2017, 4(2): 399-419.
- [13]. Hewamalage H, Bergmeir C, Bandara K. Recurrent neural networks for time series forecasting: Current status and future directions[J]. *International Journal of Forecasting*, 2021, 37(1): 388-427.
- [14]. H. Zhou *et al.*, "Informer: Beyond efficient transformer for long sequence time-series forecasting," *Proc. AAAI Conf. Artif. Intell.*, vol. 35, no. 12, 2021.
- [15]. H. Wu, J. Xu, J. Wang, and M. Long, "Autoformer: Decomposition Transformers with Auto-Correlation for Long-Term Series Forecasting," *Adv. Neural Inf. Process. Syst.*, 34, pp. 22419–22430, 2021.
- [16]. Y. Nie, N. H. Nguyen, P. Sinthong, and J. Kalagnanam, "A Time Series is Worth 64 Words: Long-term Forecasting with Transformers," *arXiv Prepr. arXiv1910.03771*, 2022.
- [17]. Garza A, Mergenthaler-Canseco M. TimeGPT-1[J]. *arXiv preprint arXiv:2310.03589*, 2023.
- [18]. Cohen N, Balch T, Veloso M. Trading via image classification[C]//*Proceedings of the first ACM international conference on AI in finance*. 2020: 1-6.
- [19]. Yang L, Fan X, Zhang Z. Your time series is worth a binary image: machine vision assisted deep framework for time series forecasting[J]. *arXiv preprint arXiv:2302.14390*, 2023.
- [20]. Dosovitskiy A, Beyer L, Kolesnikov A, et al. An image is worth 16x16 words: Transformers for image recognition at scale[J]. *arXiv preprint arXiv:2010.11929*, 2020.
- [21]. L. C. Chen, G. Papandreou, I. Kokkinos, K. Murphy, and A. L. Yuille, "Semantic image segmentation with deep convolutional nets and fully connected CRFs," *3rd Int. Conf. Learn. Represent. ICLR 2015 - Conf. Track Proc.*, vol. 40, no. 4, pp. 834–848, 2015.
- [22]. Tian Zhou, Peisong Niu, Xue Wang, Liang Sun, and Rong Jin. One fits all: Power general time series analysis by pretrained lm. *arXiv preprint arXiv:2302.11939*, 2023.
- [23]. Patro B N, Agneeswaran V S. Simba: Simplified mamba-based architecture for vision and multivariate time series[J]. *arXiv preprint arXiv:2403.15360*, 2024.
- [24]. Wu H, Hu T, Liu Y, et al. Timesnet: Temporal 2d-variation modeling for general time series analysis[J]. *arXiv preprint arXiv:2210.02186*, 2022.

Appendix

I Details of predefined prior/ empirical distributions in RealTS

This section provides comprehensive details of the predefined prior and empirical distributions utilized in RealTS. We also include parameter settings employed in our experimental section.

IFFTB Configuration: For the IFFTB, the selection of A_m and ϕ is based on empirical distributions illustrated in Figure A1. During our experiments, we randomly selected one of the two empirical distributions for generating A_m and ϕ . Detailed parameters of these distributions can be found on our GitHub repository.

PWB Configuration: The PWB primarily involves prior distributions for amplitude and frequency, represented as $P(A)$ and $P(\omega)$. In our experimental setup, their probability densities are defined as follows:

$$A \sim U(0.5, 5) \quad (A1.1)$$

$$\ln(\omega) \sim U(\ln(11), \ln(2L)) \quad (A1.2)$$

Additionally, the parameter k_{PWB} is modeled as a random variable with the following probability density:

$$P(k_{PWB} = k) = \frac{1}{8}, \text{ for } k = 1, 2, \dots, 8 \quad (A1.3)$$

LGB Configuration: The LGB includes two logistic growth function parameters: Carrying Capacity $P(K)$ and Growth Rate $P(r)$. For our experiments, we defined their probability densities as follows:

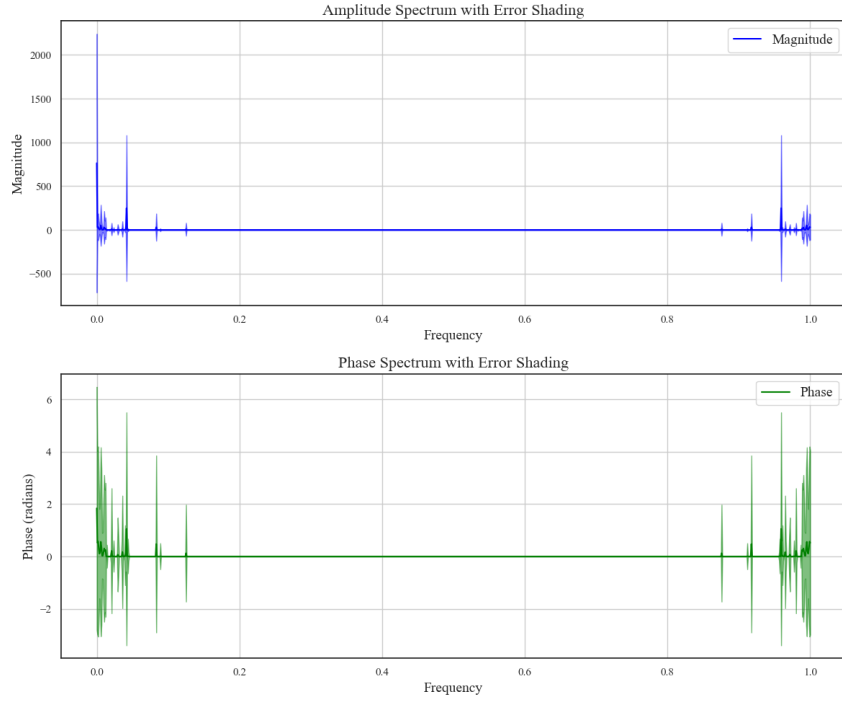
$$\ln(k) \sim U(\ln(1), \ln(10)) \quad (A2.1)$$

$$\ln(r) \sim U(\ln(0.001), \ln(0.1)) \quad (A2.2)$$

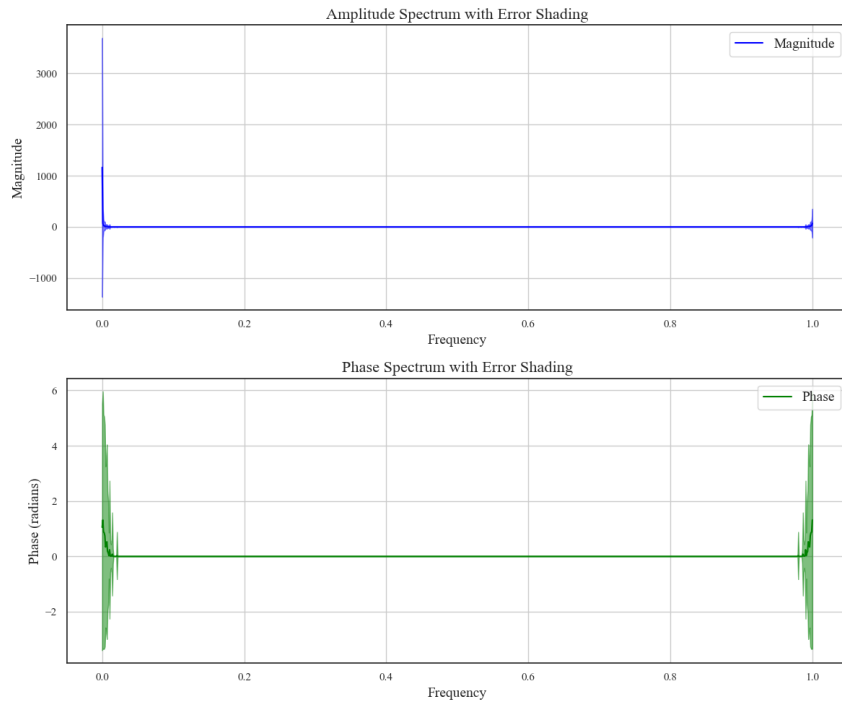
TWDB Configuration: In the TWDB, we define the probability densities for linear function random variables $P(a)$ and $P(b)$, as well as for the superimposed periodic wave components $P(A)$ and $P(\omega)$. The settings for $P(A)$, $P(\omega)$, and k_{TWDB} are consistent with those used in the PWB module. The probability densities for $P(a)$ and $P(b)$ are detailed below:

$$a \sim U(-1, 1) \quad (A3.1)$$

$$b \sim U(-10, 10) \quad (A3.2)$$



(a) Empirical distributions I in IFFTb



(b) Empirical distributions II in IFFTb.

Fig. A.1 Empirical distributions in IFFTb.

II Details of ViTime model structure

The detailed network configuration of the proposed ViTime are reported in Table A.1.

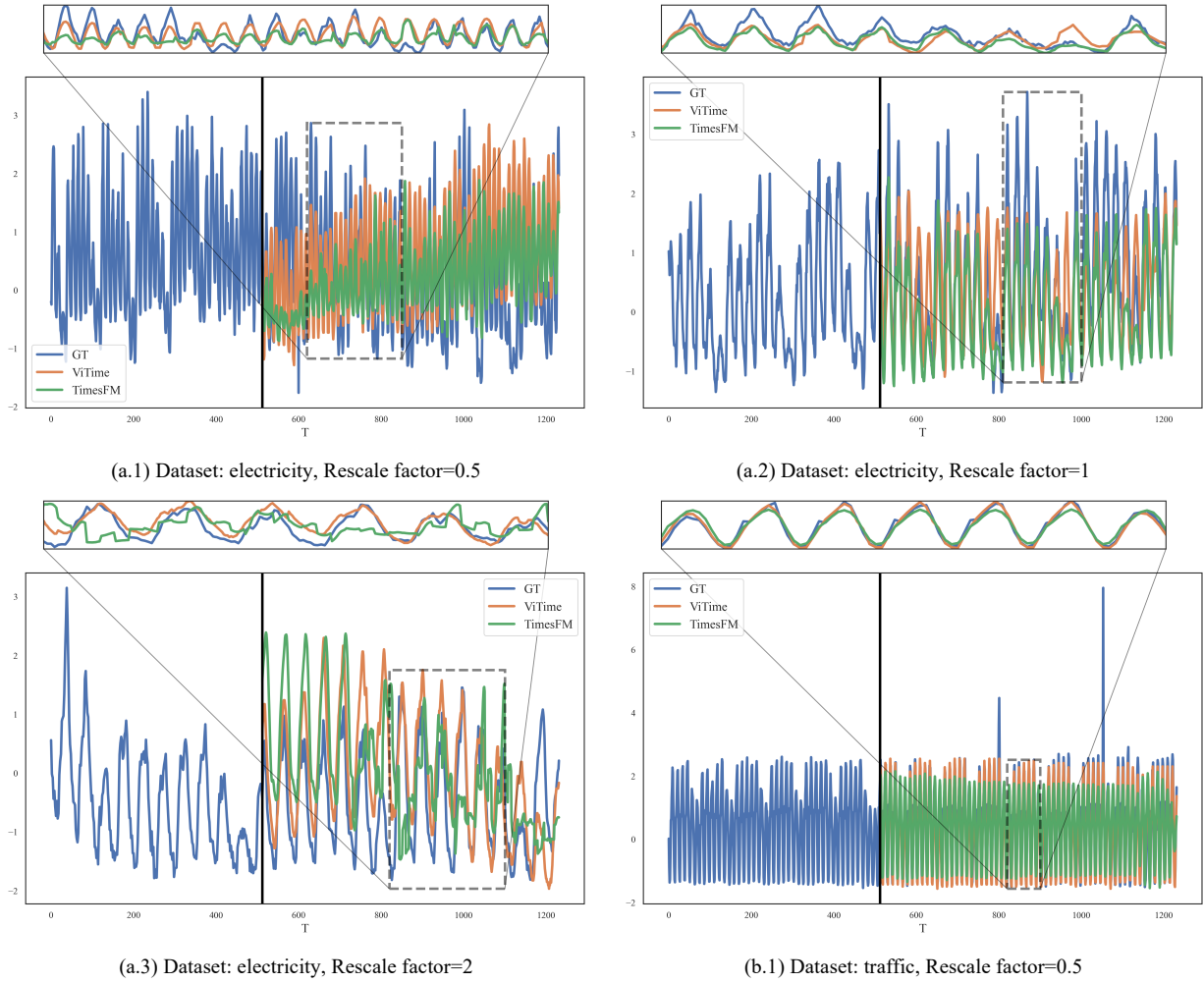
Table A.1. Details of model architecture

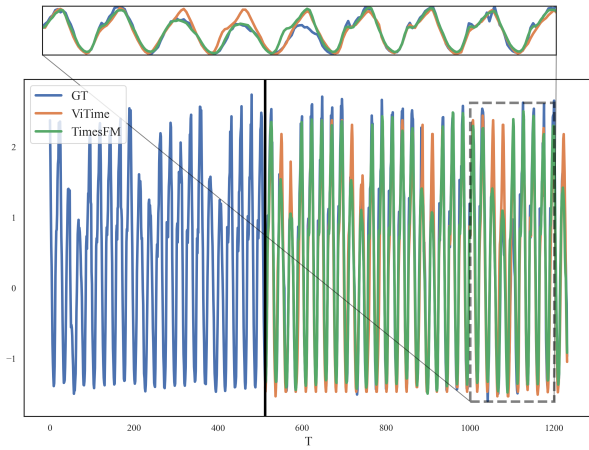
| Module | Embed_dim | Depth | Patch size | Num_heads |
|-----------------------|-----------|-------|------------|-----------|
| Visual Time Tokenizer | 768 | 9 | (4,32) | 12 |
| Decoder | 384 | 4 | \ | 12 |

For Refining Module, we set mobilenetv2 as the backbone

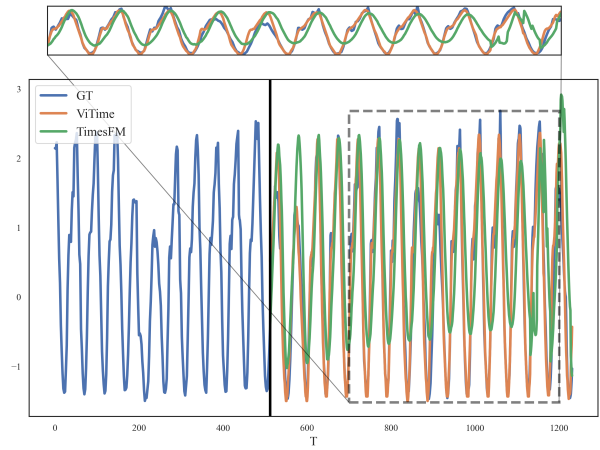
III Illustrative examples

This section presents illustrative examples of the proposed ViTime model and baseline models in zero-shot tasks. As depicted in Fig. A.2, ViTime consistently demonstrates superior zero-shot prediction performance compared to TimesFM across a range of rescale factors.

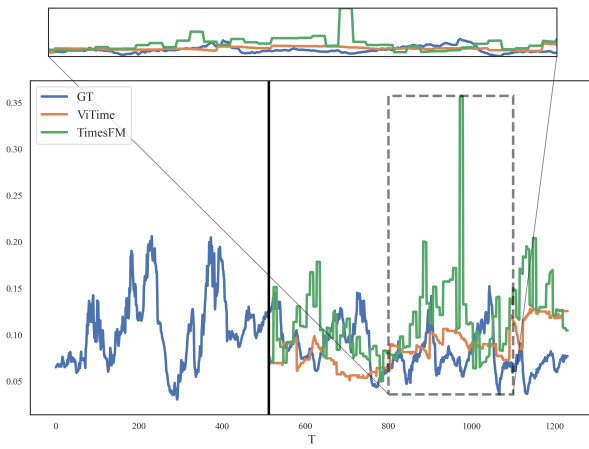




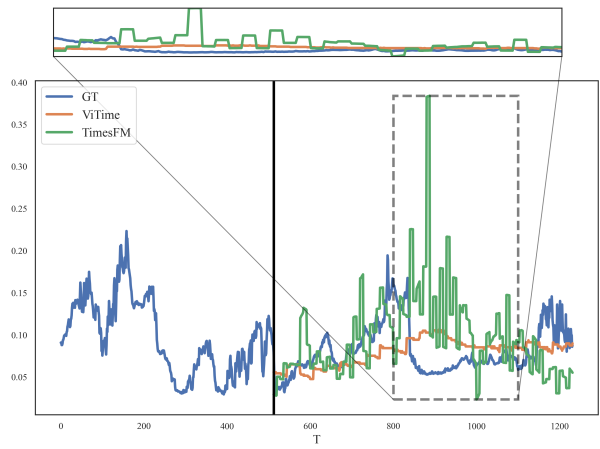
(b.2) Dataset: traffic, Rescale factor=1



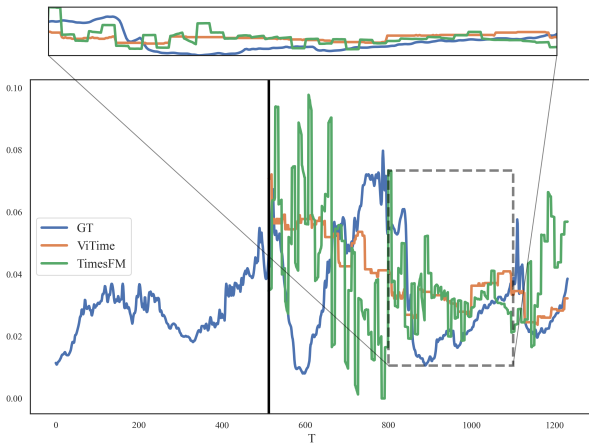
(b.3) Dataset: traffic, Rescale factor=2



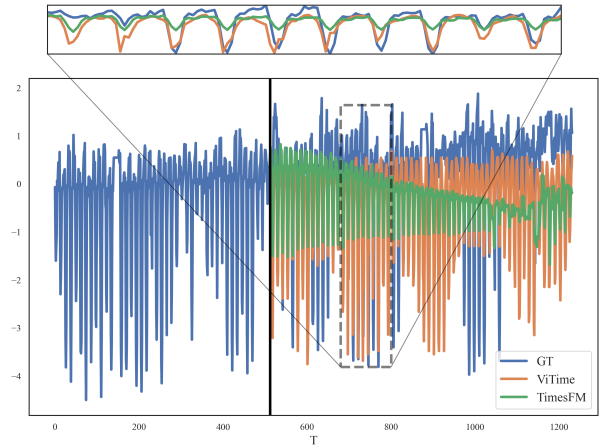
(c.1) Dataset: weather, Rescale factor=0.5



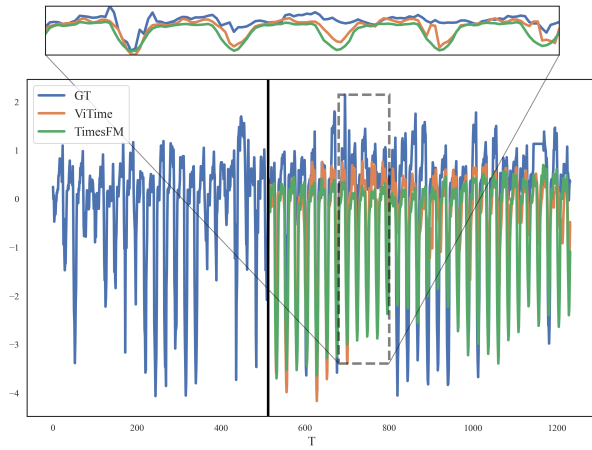
(c.2) Dataset: weather, Rescale factor=1



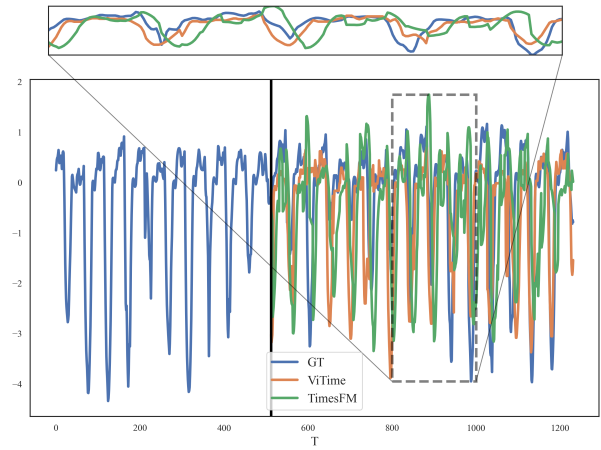
(c.3) Dataset: weather, Rescale factor=2



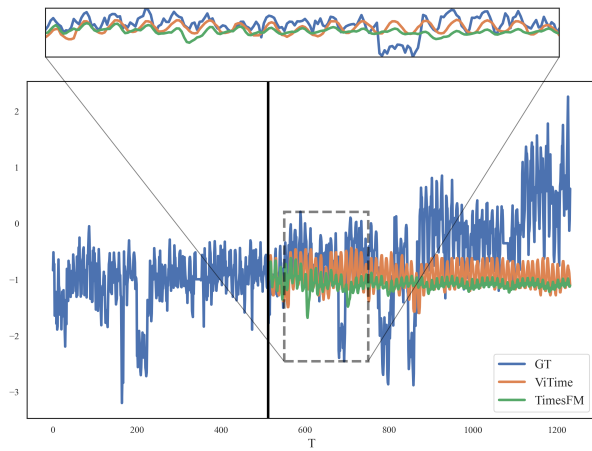
(d.1) Dataset: ETTh1, Rescale factor=0.5



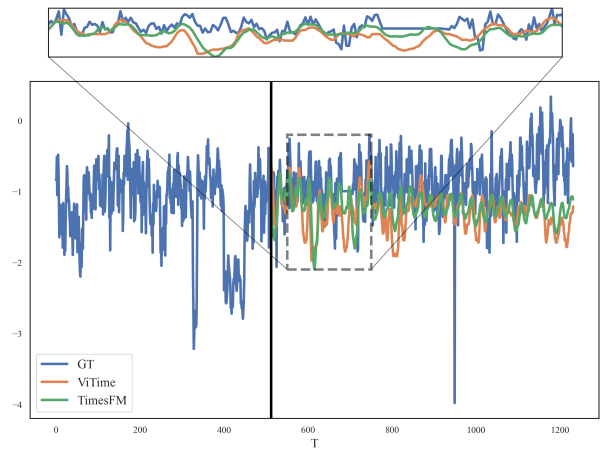
(d.2) Dataset: ETTh1, Rescale factor=1



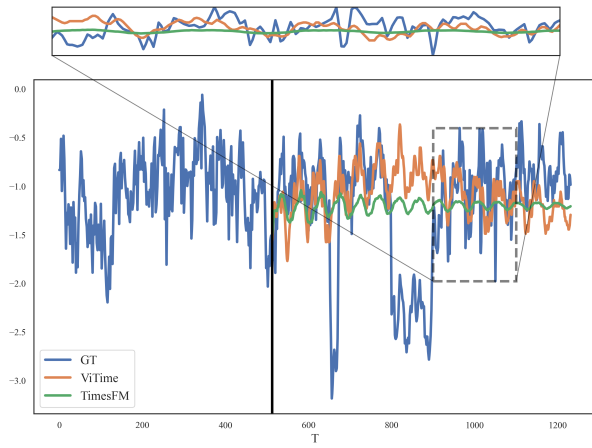
(d.3) Dataset: ETTh1, Rescale factor=2



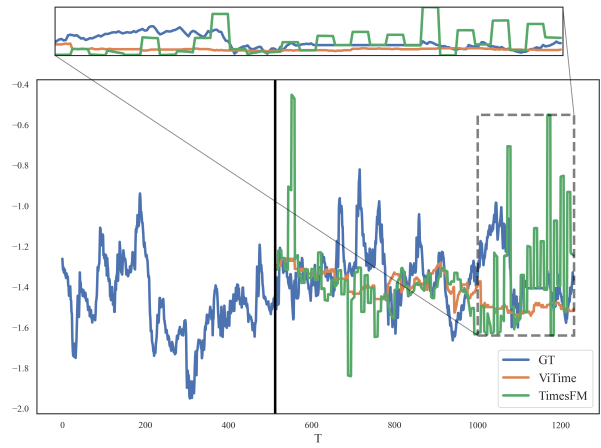
(e.1) Dataset: ETTh2, Rescale factor=0.5



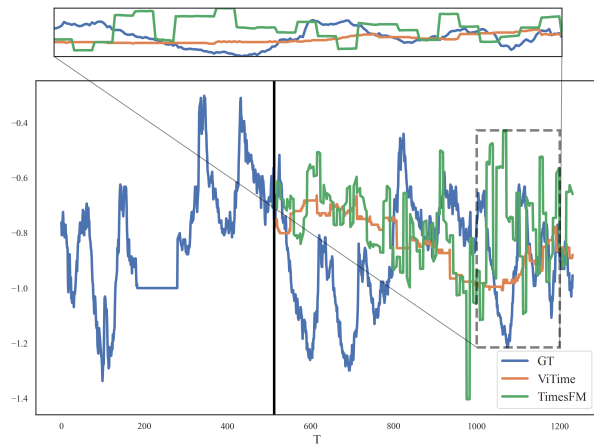
(e.2) Dataset: ETTh2, Rescale factor=1



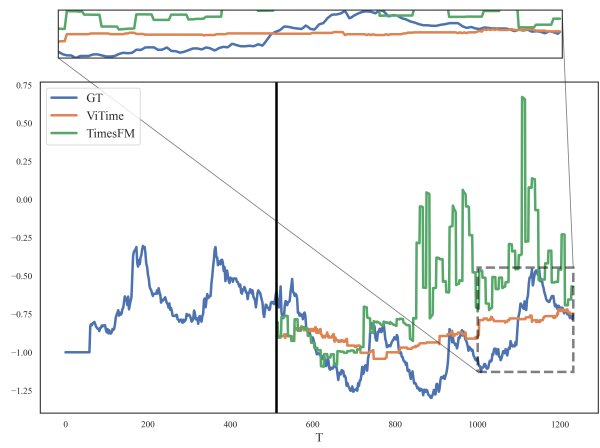
(e.3) Dataset: ETTh2, Rescale factor=2



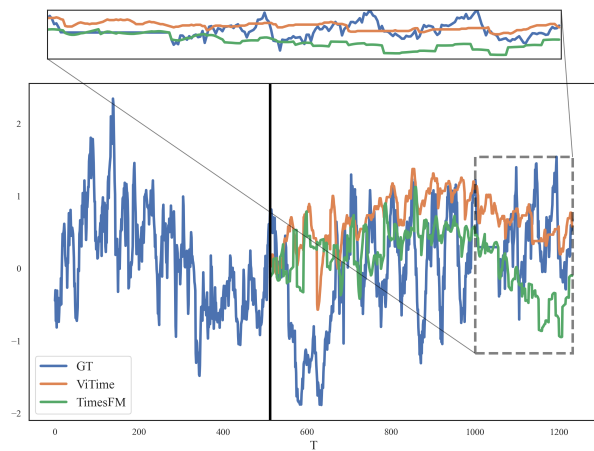
(f.1) Dataset: ETTm1, Rescale factor=0.5



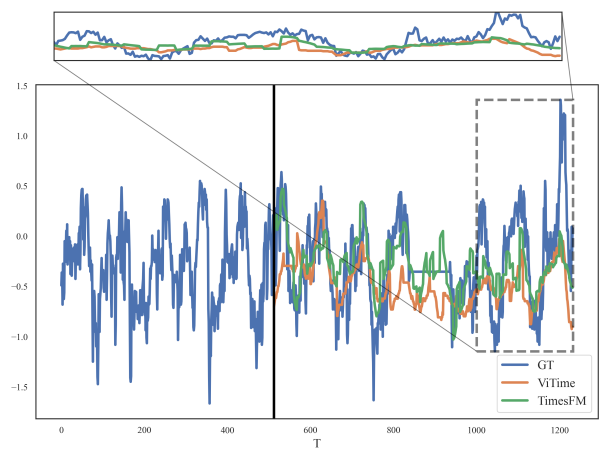
(f.2) Dataset: ETTm1, Rescale factor=1



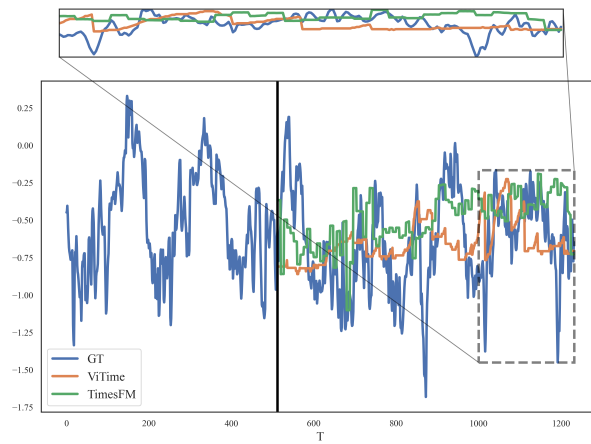
(f.3) Dataset: ETTm1, Rescale factor=2



(g.1) Dataset: ETTm2, Rescale factor=0.5



(g.2) Dataset: ETTm2, Rescale factor=1



(g.3) Dataset: ETTm2, Rescale factor=2

Fig. A.2. Illustrative example of the proposed ViTime and TimesFM with prediction length equals 720.

IV Full results of finetuning study

The detailed results of our fine-tuning study are provided in Tables A.2 and A.3.

Table. A.2. Full computational results of finetuning study

| Method | VITIME(FT) | TimesFM(FT) | GPT4TS(FT) | TIME-LLM(FT) | PatchTST | PatchTST | |
|-----------------|------------|--------------|--------------|--------------|----------|--------------|-------|
| Data proportion | 10% | 10% | 10% | 10% | 100% | 10% | |
| ETTh1 | 96 | 0.397 | 0.398 | 0.485 | 0.460 | 0.400 | 0.485 |
| | 192 | 0.414 | 0.424 | 0.524 | 0.483 | 0.429 | 0.524 |
| | 336 | 0.427 | 0.436 | 0.550 | 0.540 | 0.440 | 0.550 |
| | 720 | <u>0.460</u> | 0.445 | 0.610 | 0.604 | 0.468 | 0.610 |
| | Average | 0.424 | 0.426 | 0.542 | 0.522 | 0.434 | 0.542 |
| ETTh2 | 96 | 0.324 | 0.356 | 0.389 | 0.326 | <u>0.337</u> | 0.389 |
| | 192 | 0.354 | 0.400 | 0.414 | 0.373 | <u>0.382</u> | 0.414 |
| | 336 | 0.377 | 0.428 | 0.441 | 0.429 | <u>0.384</u> | 0.441 |
| | 720 | <u>0.431</u> | 0.457 | 0.480 | 0.449 | 0.422 | 0.480 |
| | Average | 0.372 | 0.410 | 0.431 | 0.394 | <u>0.381</u> | 0.431 |
| ETTm1 | 96 | 0.341 | 0.345 | 0.419 | 0.388 | <u>0.346</u> | 0.419 |
| | 192 | 0.364 | 0.374 | 0.434 | 0.416 | <u>0.370</u> | 0.434 |
| | 336 | 0.386 | 0.397 | 0.454 | 0.426 | <u>0.392</u> | 0.454 |
| | 720 | 0.420 | 0.436 | 0.556 | 0.476 | 0.420 | 0.556 |
| | Average | 0.378 | 0.388 | 0.466 | 0.427 | <u>0.382</u> | 0.466 |
| ETTm2 | 96 | <u>0.260</u> | 0.263 | 0.274 | 0.261 | 0.256 | 0.274 |
| | 192 | 0.293 | 0.309 | 0.317 | 0.314 | 0.296 | 0.317 |
| | 336 | 0.325 | 0.349 | 0.353 | 0.327 | <u>0.329</u> | 0.353 |
| | 720 | 0.382 | 0.415 | 0.427 | 0.390 | <u>0.385</u> | 0.427 |
| | Average | 0.316 | 0.334 | 0.343 | 0.323 | <u>0.317</u> | 0.343 |

Table. A.3. Full computational results of finetuning study

| Method | VITIME-512(FT) | SiMBA | TIMESNET | PatchTST | |
|-----------------|----------------|--------------|--------------|----------|--------------|
| Data proportion | 100% | 100% | 100% | 100% | |
| ETTh1 | 96 | 0.383 | <u>0.395</u> | 0.402 | 0.400 |
| | 192 | 0.401 | <u>0.424</u> | 0.429 | 0.429 |
| | 336 | 0.410 | <u>0.443</u> | 0.469 | 0.440 |
| | 720 | 0.438 | <u>0.469</u> | 0.500 | 0.468 |
| | Average | 0.408 | <u>0.433</u> | 0.450 | 0.434 |
| ETTh2 | 96 | 0.302 | 0.339 | 0.374 | <u>0.337</u> |
| | 192 | 0.331 | 0.390 | 0.414 | <u>0.382</u> |
| | 336 | 0.352 | 0.406 | 0.452 | <u>0.384</u> |
| | 720 | 0.411 | 0.431 | 0.468 | <u>0.422</u> |
| | Average | 0.349 | 0.393 | 0.427 | <u>0.381</u> |
| ETTm1 | 96 | 0.333 | 0.360 | 0.375 | <u>0.346</u> |
| | 192 | 0.353 | 0.382 | 0.387 | <u>0.370</u> |
| | 336 | 0.373 | 0.405 | 0.411 | <u>0.392</u> |
| | 720 | 0.410 | 0.437 | 0.450 | <u>0.420</u> |
| | Average | 0.367 | 0.396 | 0.406 | <u>0.382</u> |
| ETTm2 | 96 | 0.237 | 0.263 | 0.267 | <u>0.256</u> |
| | 192 | 0.278 | 0.306 | 0.309 | <u>0.296</u> |
| | 336 | 0.313 | 0.343 | 0.351 | <u>0.329</u> |
| | 720 | 0.371 | 0.399 | 0.403 | <u>0.385</u> |
| | Average | 0.300 | 0.327 | 0.332 | <u>0.317</u> |